9-28-2015

3D Printed Microtransporters: Compound Micromachines for Spatiotemporally Controlled Delivery of Therapeutic Agents

Tian-Yun Huang

Mahmut Selman Sakar

Angelo Mao

Andrew Petruska

Xue-Bo Chen

See next page for additional authors

Citation/Publisher Attribution

Huang, T. , Sakar, M. S., Mao, A. , Petruska, A. J., Qiu, F. , Chen, X. , Kennedy, S. , Mooney, D. and Nelson, B. J. (2015), 3D Printed Microtransporters: Compound Micromachines for Spatiotemporally Controlled Delivery of Therapeutic Agents. Adv. Mater., 27: 6644-6650. doi:10.1002/adma.201503095
Available at: http://dx.doi.org/10.1002/adma.201503095

Submitted to ADVANCED MATERIALS
DOI: 10.1002/adma.((please add manuscript number))

Wirelessly powered compound micromachines for triggered and targeted interventions

By *Tian-Yun Huang, Mahmut Selman Sakar*, Angelo Mao, Andrew Petruska, Xue-Bo Chen, Stephen Kennedy, David Mooney, and Bradley J. Nelson*

[*]Tian-Yun Huang, Dr. Mahmut Selman Sakar, Dr. Andrew Petruska, Prof. Bradley Nelson
Institute of Robotics and Intelligent Systems
ETH Zurich, Zurich, CH 8092, Switzerland
Email: sakarm@ethz.ch

Prof. Stephen Kennedy
Department of Electrical, Computer, and Biomedical Engineering
Department of Chemical Engineering
University of Rhode Island
Kingston, RI 02881

Angelo Mao, Prof. David Mooney
Wyss Institute for Biologically Inspired Engineering
School of Engineering and Applied Sciences, Harvard University,
Cambridge, MA 02318, USA

Tian-Yun Huang, Prof. Xue-Bo Chen
School of Electronics and Information Engineering
Liaoning University of Science and Technology
Anshan, 114051, China

Keywords: microrobotics, micromachines, 3D printing, targeted drug and cell delivery, magnetism

Biological systems are exquisitely sensitive to the location, dose, and timing of physiologic cues and drugs. This spatiotemporal sensitivity indicates that diagnostic and therapeutic approaches with minimal off-target effects can be particularly efficacious. Untethered, miniaturized robotic devices can enable us to perform minimally invasive operations in three-dimensional, complex microenvironments.[1,2] Critically, these remotely actuated operations can potentially be performed in order to perturb or investigate biological systems in a flexible and on-demand manner. A variety of simple micromachines have recently been developed including microstructures controlled by oscillating magnetic fields,[3-5] helical swimmers demonstrating corkscrew motion,[6] thermally or magnetically actuated microgrippers,[7-10] self-propelled micromotors,[11] electrostatic[12] and impact-driven microactuators.[13] These machines can transport cargo by forming a physical contact with the manipulated objects and/or by utilizing the fluid flow generated around their body.[14-19] The diagnostic and therapeutic potential of robotics in these micro-biological contexts can be greatly enhanced with the development of compound micromachines that have multiple mechanisms working together to perform complicated tasks.

Targeted delivery of drugs, genetic material, and cells increase the effectiveness of therapies while minimizing side effects.[20] Several micro- and nano-particles have been developed to safely carry these therapeutic payloads.[21,22] Systemic injection of these particles results in their dilution and only a small fraction of the particles reaches the treatment region. Magnetic targeting actively enhances the deposition of particles at the target locations and significantly increases the delivered dose compared to passive diffusion.[23] However, explicit visualization, navigation, and controlled introduction of individual nanoagents to target sites within complex biological systems is challenging due to their small size and weak magnetization. Furthermore, hostile environmental conditions, physical barriers, and the immune system can eliminate them. Thus, for therapeutic purposes, the current challenge is to engineer a protective capsule that can retain its payload during transport and then controllably release its contents at the target site in a dose-dependent manner. For diagnostic purposes, capsules could be utilized to collect biological samples from remote pathological sites without using invasive procedures.

Stimuli responsive mobile microcapsules have been introduced to address these challenges,[9,24] but they release their payload en masse and do not have an active loading or mixing mechanism.

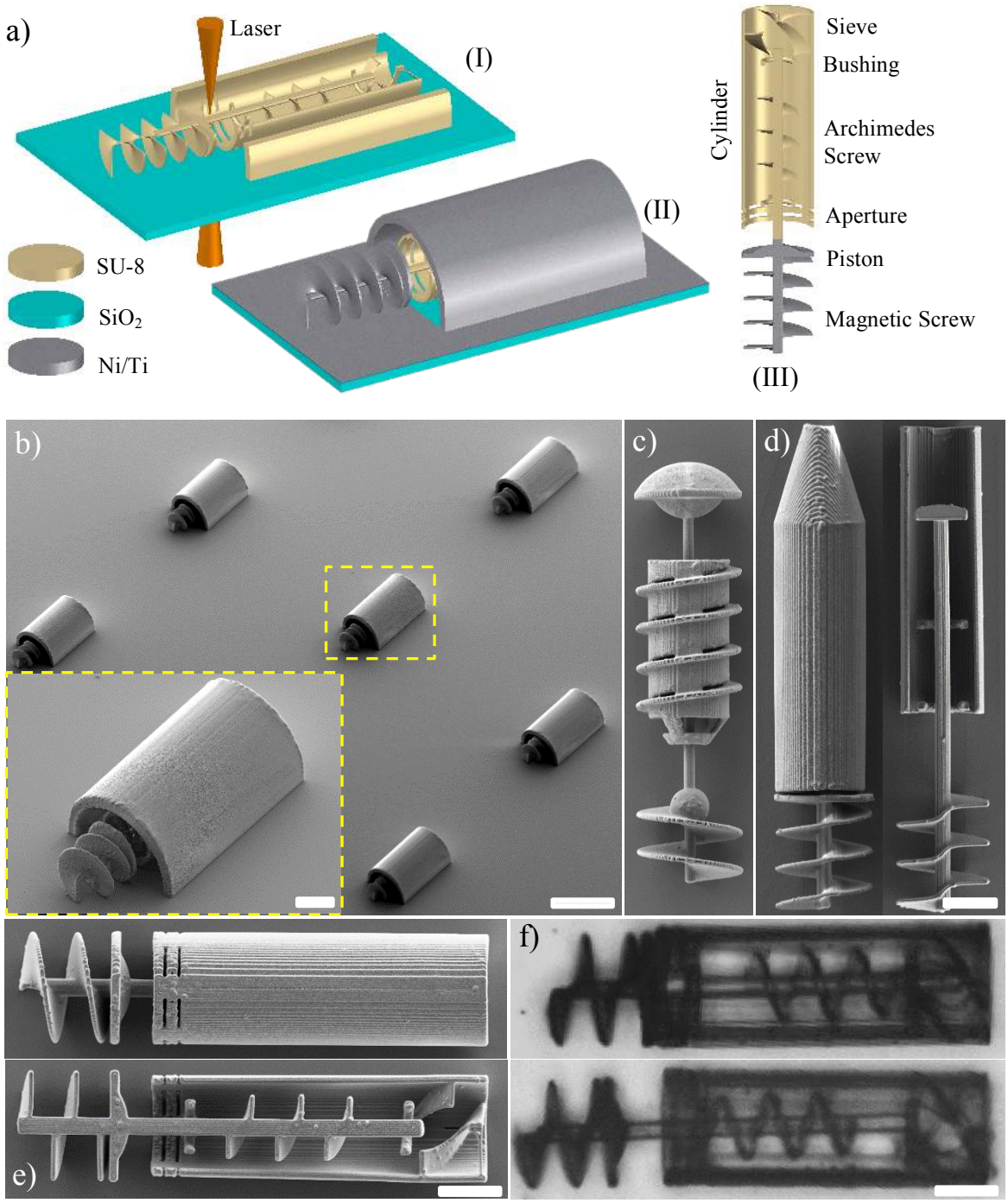

Figure 1. a) Schematic description of fabrication process: (I) 3-D laser direct writing of microstructures, (II) Selective physical vapour deposition, (III) The final product illustrating different mechanical components of the micromachines. b) A horizontal array of micromachines before the

removal of sacrificial components. The scale bars are 20 μm and 100μm. c-d) Micromachines designed to transport mass using the reciprocating mechanism either by using capsules (c) or syringes with movable plungers (d). e) The full and cross-sectional view of the final prototype with engineered propeller. f) Two open and close modes of the reciprocating mechanism. The main shaft translates due to the rotation of the screw. The scale bars in (c)-(f) are 20 μm.

Here, we report a design methodology to fabricate compound micromachines using three dimensional (3D) direct laser writing and selective physical vapor deposition of magnetic materials (**Figure 1**a). Laser lithography offers excellent control over the 3D geometry as well as high resolution for engineering intricate parts. The fabrication process allows us to directly print custom shaped microparts to create a unified body without further assembly (Figure 1a(I)). To fabricate an integrated mechanical system with parts that must move relative to each other, it is important to generate magnetic actuation only at specific locations. To perform selective coating of magnetic materials, we printed 3D sacrificial structures to protect all the parts except the outer screw during Ni/Ti metal deposition (Figure 1a(II)). Figure 1b shows SEM images of micromachines along with surrounding sacrificial structures. These structures were removed using a sharp probe controlled by a micromanipulator after the deposition process. A schematic diagram of the individual parts of the micromachine is shown in Figure 1a(III). The devices consist of a main shaft embedded inside a cylindrical capsule. The shaft is free to rotate, and its translation is constrained at both ends of the capsule by the circular bushings. The magnetic screw generates corkscrew motion in the presence of a rotating magnetic field. While the corkscrew motion results in the translation of the whole device for targeted therapy, it also controls the action of the tools attached to the shaft for triggered operations. Thus, the positioning of this device and its shaft's rotation can be controlled together using external magnetic signals. In this work, we concentrate on the spatiotemporally controlled collection, transport and release of hundreds of polystyrene and alginate microparticles as well as magnetic nanohelices inside microfluidic channels.

We engineered microcapsules with removable caps (Figure 1c) and microsyringes with sliding plungers (Figure 1d). The caps can be repeatedly closed and opened, and the plunger can be moved back and forth by reversing the magnetic field's rotation. However, at the microscale, capturing and releasing payloads with only a physical push is highly ineffective due to viscous forces and surface adhesion (see Figure S1). Furthermore, tightly sealed plunger type structures cannot be effectively operated due to high friction between the capsule and the plunger. Previous work has shown that a microvortex generated by a rotating object can be used to effectively trap and transport individual microparticles.[17-19] However, strategies such as these cannot be applied to delivering multiple particles, and the trapped particle is susceptible to environmental disturbance during transport.

To address these problems, we engineered an Archimedes screw pumping mechanism by engraving a second screw onto the main shaft (Figure 1e). Figure 1f shows the translational motion of the main shaft inside the capsule. The rotating screw draws fluid and particles into the capsule while the piston slides forward to close the rear part of the capsule and trap the particles within (**Figure 2**). When actuated in reverse, the piston slides into the open configuration, and the trapped particles are gradually expelled with the reverse flow generated by the propeller. We engineered three microblades, forming an equilateral triangle in the front of the capsule, to form a sieve (see Figure 1a(III)). The sieve, together with the apertures printed at the rear part of the capsule and on the piston (see Figure S2), function as filters to select particles within the desired size range while allowing the fluid flow through the body.

The schematic diagram in Figure 2a summarizes the remotely activated loading and releasing process (Supplementary Movie 1). The microparticles, drawn into the chamber by the recirculating flow induced by the micropump (Figure 2b), stay inside the capsule as the tail closed the rear side at this stage. As expected, the strongest pumping action is generated when the capsule body is immobilized while driving the screws (Supplementary Movie 2). The screws were designed to rotate freely, but the capsule starts rotating sympathetically from fluidic forces and from part-to-part contacts during operation. On a planar surface, due to surface adhesion, the capsule motion was limited. To further

minimize the rotation of the capsule during loading, the propeller was operated at frequencies below 15Hz. The capsules are optically transparent; therefore, we could visualize the internal content using brightfield or phase-contrast imaging (Figure 2c).

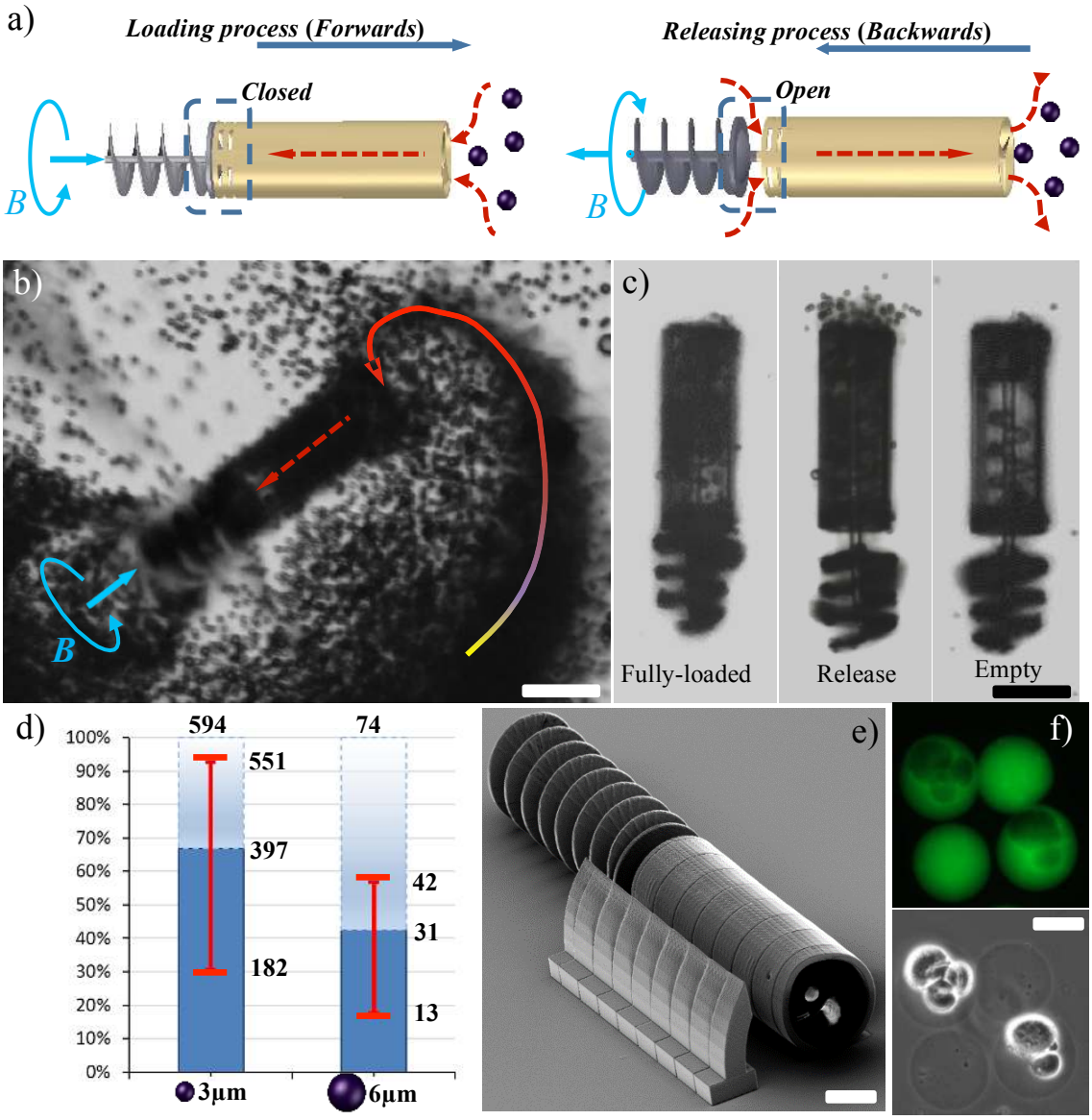

Figure 2. a) Schematic description of the loading and releasing mechanism. b) The remotely actuated rotation of the screw generates a fluid flow around the micromachine that goes through the capsule, which leads to the loading of polystyrene microbeads (3µm diameter). c) Sequence of images summarizing the release process. A micromachine (I) fully-loaded with particles, (II) in the beginning of the release process, (III) at the end of the release process. d) The loading capacities of the engineered micromachine for 3µm and 6µm beads. 100% marks the total volume of the micromachine. e) An up-scaled prototype was fabricated to transport cell-loaded alginate microbeads. (f) Cell encapsulation inside alginate microbeads. Fluorescence (green, top panel) and differential interference

contrast (DIC) image (bottom panel) shows the microbeads and the encapsulated cells. All scale bars are 50μm.

Figure 2c shows a loaded micromachine before, during, and after the release process. The machines were actuated with a rotating magnetic field of 9mT at varying frequencies. The loading capacity is evaluated for two different polystyrene microspheres 3μm and 6μm in diameter (Figure 2d). The maximum number of beads that can be fitted into a capsule, N_{bead}, can be calculated as

$$N_{bead} = \mu_{max} \cdot \frac{C_{machine}}{V_{bead}} \quad (1)$$

The total volume of the micromachine $C_{machine} \approx 90827\mu m^3$, the volume of the microbead $V_{bead} = (4/3)\pi r^3$ and $\mu_{max}$is the greatest fraction of space occupied by equal microspheres for the hexagonal close-packed structure, which is given by

$$\mu_{max} = \frac{N_{sphere} \cdot V_{sphere}}{V_{unitcrystal}} = \frac{6 \cdot (4/3)\pi r^3}{[(3\sqrt{3})/2](\sqrt{\frac{2}{3}})(16r^3)} = \frac{\pi}{3\sqrt{2}} \approx 0.74 \quad (2)$$

N_{bead} values for 3μm and 6μm beads are 594 and 74, respectively.

Processing images of several fully loaded micromachines showed that the smaller beads were captured more efficiently (67% average) than larger beads (41% average). Larger beads occasionally clog the passage, disrupting the pumping mechanism. At high concentrations, the trapped particles cause jamming, and the rotation of the capsule couples with the rotation of the shaft. This synchronous motility impedes the active transport of the particles and the sieve minimizes the diffusion of particles from the capsule. As a result, most of the microbeads remained inside the capsule throughout the transport missions, which would be valuable in therapeutic delivery and diagnostic recovery applications. The encapsulated particles were released with the reversal of the flow generated by the clockwise rotation of the shaft. The microparticles were pushed out with an average flow rate of 9.2 pL/sec at 10Hz. At this flow rate the loaded capsule can be completely emptied in less than 10 seconds. The flow rate can be adjusted by modulating the rotating speed of the magnetic field. The delivered dose of particles depends on the flow rate and the duration of counterclockwise rotation of the screw. As the process is reversible, the screw can be rotated in a clockwise direction to collect some of the released particles back into the capsule for fine adjustment of the dose (See Supplementary Movie 3).

Cell injection therapies are occasionally hampered due to the lack of control to direct their localization. Infused cells are often trapped in the lungs or other organs.[27] While antibody strategies partially address this problem, an active guidance and delivery platform could significantly improve the homing of cells at the injury sites. In our previous work, we showed that use of a Ni/Ti coating on the printed microstructures does not induce cytotoxicity to mammalian cells after days of exposure, and the cells readily adhere and proliferate over the devices.[28] In this work, we applied an additional polyethylene glycol (PEG) coating on the outer surface of the micromachine to hide the agent from the host's immune system and minimize protein accumulation, thus making them more compatible with bodily fluids and the tissue microenvironment. Directly loading cells into the capsules has several drawbacks. First, they start adhering to the interior surface of the capsule and each other, which leads to the formation of cell agglomerates. Preventing this adhesion with surfactants results in cell death as the transport tasks can take minutes to hours. Furthermore, the Archimedes screw applies high shear stress on the cells during loading and release.

Biodegradable alginate microbeads can be formed using a sterile process with relatively mild pH and temperature conditions allowing for long-term and sustained delivery of both drugs and cells.[29] We fabricated alginate microbeads with diameters ranging from 10 to 60 μm using a microfluidic cross-junction device (see Figure S3). To test the possibility of targeted cell-based therapeutics, live mammalian cells were encapsulated inside the microbeads (**Figure 2**f). The encapsulated cells stay viable for days under physiological conditions.[8] The dimensions of the compound micromachine had to be scaled up to transport alginate microbeads with relatively larger sizes compared to the PS beads and single cells (**Figure 2**e). We increased the number of turns in the magnetic screw to generate stronger fluid flows. The developed prototype can successfully encapsulate and transport several alginate beads (see Supplementary Movie 4). We did not observe any visible plastic deformation on the soft bodies, and the beads did not adhere to the internal surface of the capsule. Due to their transparency, fluorescence microscopy greatly aids the visualization of microbeads (Figure 2f).

In our previous work we showed that magnetic nanohelices can be used for targeted drug and gene delivery in vitro and in vivo.[30-32] Swarms of functionalized helical swimmers could lead to more effective therapies due to their active transport capability.[32] However, they still face the issues related to systemic dilution and active elimination when injected as a suspension. Using the compartmentalization concept, we tested if compound micromachines could be employed as motherships to transport smaller microswimmers (**Figure 3**). The helical structures were designed with left-handed chirality as opposed to the right-handed chirality of the micromachine's screw to force helices and compound micromachines to swim towards each other during loading and in the opposite direction during release. After loading, the micromachines can successfully transport several microswimmers. We fabricated a microfluidic channel with three branches to create an artificial capillary network. The loaded micromachines were successfully guided into the main channel and the released tiny microswimmers were navigated further to the smaller branches (see Supplementary Movie 5). The process of targeted delivery with compartmentalization is demonstrated in Figure 3b-d. Due to their size and magnetization, the helical microstructures swim slower than compound micromachines (Figure 3e).

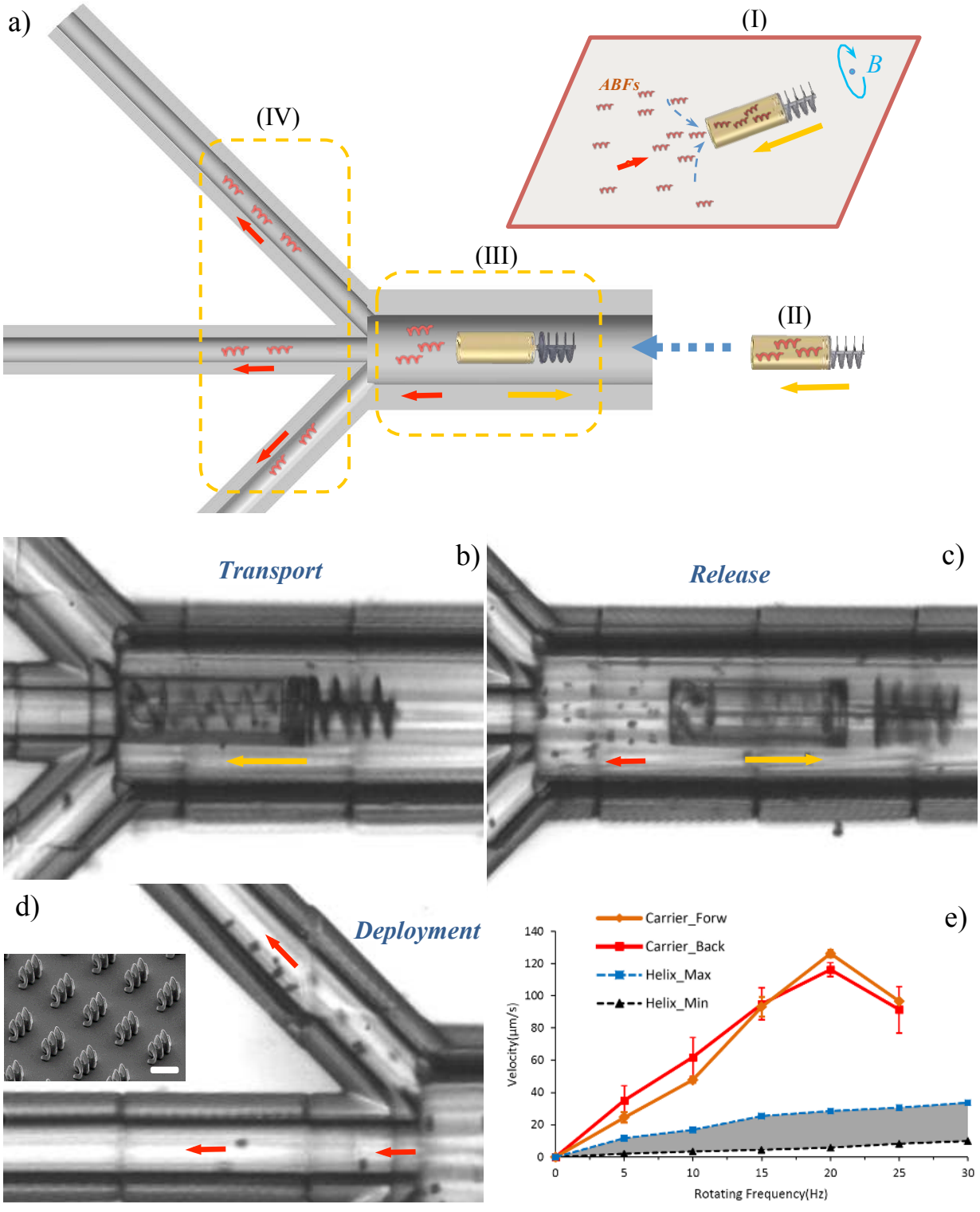

Figure 3. a) Different stages of the transport and delivery of tiny helical microstructures using the compound micromachine: (I) Loading, (II) Transport, (III) Release, and (IV) Deployment. b) We have successfully transported helices inside microfluidic channels. c) Helices were released at the target location with reversal of the screw rotation. Due to change in charality, the magnetic helices swam forward while the micromachine swam backwards. d) Swarms of microhelices were directed to move into the narrower branches. The inset shows an SEM image of an array of helical microstructures. The

scale bar is 2 μm. e) Velocity profile of the compound micromachine and helical microstructures with increasing rotating frequencies.

The frequency at which the maximum forward velocity is achieved is known as step-out frequency and the machine's velocity rapidly declines when operated above that level. The step-out frequency depends on many parameters such as friction and the magnetization of the structures, which change significantly with size and design of the structures. The compound machines reach step-out around 20Hz at 9mT while the velocity of microswimmers monotonically increases until 100Hz. Within this window (20Hz-100Hz), the frequency of rotating magnetic field can be modulated to disable the motility of micromachines while moving the swimmers toward their target locations. Inside the confined volume of the capsule, the microhelices can form agglomerates. However, the rotational motion of the shaft along with the propeller and the fluidic forces separated such clusters during release process. Previous work has shown that magnetic attraction can induce the assembly of helices during collective swimming, whereas fluidic forces disassemble them or limit the size of the assembly.[33] In our experiments, under rotating frequencies above 60Hz, fluidic forces among microhelices were strong enough to avoid formation of large clusters. This approach is not limited to the transport of particles, cell-loaded microcarriers and magnetic nanohelices; other passive and active suspensions (i.e. suspensions of self-propelling catalytic motors[10]) can be transported inside selected microfluidic systems.

We introduce the design and fabrication of compound micromachines for targeted and triggered delivery of particles, biological materials and smaller micromachines. Functional microparts were printed together to form a single device without the need for further assembly using direct laser writing and selective magnetic film deposition. A pumping mechanism based on rotational motion of propellers is engineered to load and release cargo in a dose-dependent manner. We demonstrate the delivery of swarms of tiny helices inside microfluidic channels, the propulsion of such teams into even smaller cavities, and independent/reverse movement of these teams and their mothership micromachine. This design methodology can be used to deliver biological payloads such as drugs and cells with a high degree of spatiotemporal precision and can also be employed to perform more

complicated tasks such as mechanical removal of occlusions, collection of biological samples for diagnostic analysis and generation of local fluid flows for mixing.

Experimental Section

Fabrication of compound micromachines and microfluidic channels: The micromachines are fabricated in the horizontal manner with SU-8 photoresist using 3D direct laser writing (The Photonic Professional Laser Lithography System, Nanoscribe GmbH) as shown in **Figure 1**a. This technique works well with the Galvo (Layer by Layer) Scanning Writing Mode and offers a good adhesion to the surface of the substrate during development. After development, 300nm thickness Ni/Ti bilayers are deposited only on the outer propeller using Physical Vapor Deposition (PVD). The microfluidic channel and helical microswimmers were printed independently. See Supplementary Table S1 for the dimensions of all the fabricated structures measured from SEM images. A high concentration suspension of helical structures coated with 50nm thick Ni/Ti bilayers were formed using tip sonication.[31] Just before the experiments, 0.1mL of Surface Active Agent (TEEN 20) was used to lubricate the junctions of mechanical components, and the solution was degassed for five minutes to release air bubbles trapped in the capsules. The micromachines were detached from the glass substrate and transported to the experimental chamber using a Tungsten probe with a sharp tip.

Magnetic manipulation system: Detailed information about the magnetic manipulation system can be found in our previous work.[19] The system consists of three pairs of stationary electromagnetic Helmholtz coils and is capable of producing uniform magnetic fields up to 10 mT and at frequencies up to 200 Hz. The micromachines and channels are immersed with deionized (DI) water inside a plastic reservoir (35mm×35mm×3mm), which is always placed at the center of the magnetic coils. Using this setup, the motion of the micromachine can be controlled in 3D. The system also allows the use of a conical rotating field to minimize the hydrodynamically-induced wobbling.[19]

Fabrication of the alginate microbeads: Sodium alginate was purchased from FMC Biopolymer (Princeton, NJ). Calcium carbonate nanoparticles (CalEssence(R) 70 PCC) were suspended in

complete Dulbecco's Modified Eagle Media (Sigma-Aldrich, St. Louis, MO) and either combined with alginate alone or with a suspension of K562 leukemia cells (ATCC) in alginate to make empty alginate beads or cell-encapsulating alginate beads, respectively. The continuous phase was prepared by mixing 1% fluorosurfactant[34] and sterile-filtered 0.31% acetic acid (EMD Chemicals, Gibbstown, NJ) in a fluorinated oil (3M™ Novec™ Engineering Fluid HFE-7500). The continuous and aqueous phases were injected into a cross-junction microfluidic for form a water-in-oil emulsion (see Figure S3). Emulsions were broken after a 30 minute incubation by the addition of 20% 1H,1H,2H,2H-perfluorooctanol (Alfa Aesar, Ward Hill, MA).

Supporting Information

Supporting Information is available from the Wiley Online Library or from the author.

Acknowledgements

This work was financially supported by the European Research Council Advanced Grant "Microrobotics and Nanomedicine (BOTMED)", the Swiss National Science Foundation, China Scholarship Council and National Natural Science Foundation of China (71371092). The authors are thankful to Famin Qiu, Yun Ding, Andre Lindo, Dr. Qi Zhang, and Dr. ChengZhi Hu for the assistance in experiments and the FIRST lab of ETH Zurich for technical support.

Received: ((will be filled in by the editorial staff))
Revised: ((will be filled in by the editorial staff))
Published online: ((will be filled in by the editorial staff))

[1] B. J. Nelson, I. K. Kaliakatsos, J. J. Abbott, *Annu. Rev. Biomed. Eng.* **2010**, 12, 55.
[2] M. Sitti, H. Ceylan, W. Hu, J. Giltinan, M. Turan, S. Yim, E. Diller, *Proc. IEEE* **2015**, 103, 205.
[3] S. Floyd, C. Pawashe, M. Sitti, *IEEE T. Robot.* **2009**, 25, 1332.
[4] M. S. Sakar, E. B. Steager, D. H. Kim, M. J. Kim, G. J. Pappas, V. Kumar, *Appl. Phys. Lett.* **2010**, 96, 043705.
[5] W. Jing, N. Pagano, D. J. Cappelleri, *Appl. Phys. Lett.* **2009**, 94, 064107.
[6] K. E. Peyer, S. Tottori, F. Qiu, L. Zhang, B. J. Nelson, *Chem. Eur. J.* **2013**, 19, 28.
[7] E. Gultepe, J. S. Randhawa, S. Kadam, S. Yamanaka, F. M. Selaru, E. J. Shin, A. N. Kalloo, D. H. Gracias, *Adv. Mater.* **2013**, 25, 514.
[8] T. G. Leong, C. L. Randall, B. R. Benson, N. Bassik, G. M. Stern, D. H. Gracias, *Proc. Natl. Acad. Sci. USA* **2009**, 106, 703.
[9] S. Fusco, M. S. Sakar, S. Kennedy, C. Peters, R. Bottani, F. Starsich, A. Mao, G. A. Sotiriou, S. Pane, S. E. Pratsinis, D. Mooney, B. J. Nelson, *Adv. Mater.* **2014**, 26, 952.
[10] E. Diller, M. Sitti, *Adv. Funct. Mater.* **2014**, 24, 4397.
[11] D. Patra, S. Sengupta, W. Duan, H. Zhang, R. Pavlick, A. Sen, *Nanoscale* **2013**, 5, 1273.
[12] B. R. Donald, C. G. Levey, C. McGray, I. Paprotny, D. Rus, *J. Microelectromech. Syst.* **2006,** 15, 1.
[13] D. R. Frutiger, K. Vollmers, B. E. Kratochvil, B. J. Nelson, *Int. J. Rob. Res.* **2010**, 29, 613.
[14] L. Zhang, K. E. Peyer, B. J. Nelson, *Lab Chip* **2010**, 10, 2203.
[15] M. Hagiwara, T. Kawahara, Y. Yamanishi, T. Masuda, L. Feng, F. Arai, *Lab Chip* **2011**, 11, 2049;
[16] E. B. Steager, M. S. Sakar, C. Magee, M. Kennedy, A. Cowley, V. Kumar, *Int. J. Rob. Res.* **2013**, 32, 346.
[17] H.-W. Tung, K. E. Peyer, D. F. Sargent, B. J. Nelson, *Appl. Phys. Lett.* **2013**, 103, 114101.
[18] Z. Ye, M. Sitti, *Lab Chip* **2014**, 14, 2177.
[19] T.-Y. Huang, F. Qiu, H.-W. Tung, X.-B. Chen, B. J. Nelson, M. S. Sakar, *Appl. Phys. Lett.* **2014**, 105, 114102.
[20] C. Sawyers, *Nature* **2004**, 432, 294.
[21] K. Riehemann, S. W. Schneider, T. A. Luger, B. Godin, M. Ferrari, H. Fuchs, *Angew. Chem. Int. Edit.* **2009**, 48, 872.
[22] O. C. Farokhzad, R. Langer, *ACS Nano* **2009**, 3, 16.
[23] B. Shapiro, S. Kulkarni, A. Nacev, A. Sarwar, D. Preciado, D. A. Depireux, *Annu. Rev. Biomed. Eng.* **2014**, 16, 455.
[24] S. Pedron, S. van Lierop, P. Horstman, R. Penterman, D. J. Broer, E. Peeters, *Adv. Funct. Mater.* **2011**, 21, 1624.
[25] S. Zakharchenko, N. Puretskiy, G. Stoychev, M. Stamm, L. Ionov, *Soft Matter* **2010**, 6, 2633.
[26] J. C. Breger, C. Yoon, R. Xiao, H. R. Kwag, M. O. Wang, J. P. Fisher, T. D. Nguyen, D. H. Gracias, *ACS Appl. Mater. Interfaces* **2015**, 7, 3398.
[27] T. J. Kean, P. Lin, A. I. Caplan, J. E. Dennis, *Stem Cells Int.* **2013**, 732742.
[28] S. Tottori, L. Zhang, F. Qiu, K. K. Krawczyk, A. Franco-Obregon, B. J. Nelson, *Adv. Mat.* **2012**, 24, 811.
[29] G. G. d'Ayala, M. Malinconico, P. Laurienzo, *Molecules* **2008**, 13, 2069.
[30] R. Mhanna , F. Qiu , L. Zhang , Y. Ding , K. Sugihara , M. Zenobi-Wong , B. J. Nelson, *Small* **2014**, 10, 1953.

[31] F. Qiu, S. Fujita, R. Mhanna, L. Zhang, B. R. Simona, B. J. Nelson, *Adv. Funct. Mater.* **2015**, 25, 1666–1671.
[32] A. Servant, F. Qiu, M. Mazza, K. Kostarelos, B. J. Nelson, *Adv. Mater.* **2015**, DOI: 10.1002/adma.201404444
[33] S. Tottori, L. Zhang, K. E. Peyer, B. J. Nelson *Nano Lett*. **2013**, 3, 4263-4268.
[34] C. Holtze et. al., *Lab Chip* **2008**, 8.

Submitted to ADVANCED MATERIALS

Supporting Information

Wirelessly powered compound micromachines for triggered and targeted therapeutics

By *Tian-Yun Huang, Mahmut Selman Sakar*, Angelo Mao, Andrew Petruska, Xue-Bo Chen, Stephen Kennedy, David Mooney, and Bradley J. Nelson*

[*]Tian-Yun Huang, Dr. Mahmut Selman Sakar, Dr. Andrew Petruska, Prof. Bradley Nelson
Institute of Robotics and Intelligent Systems
ETH Zurich, Zurich, CH 8092, Switzerland
Email: sakarm@ethz.ch

Prof. Stephen Kennedy
Department of Electrical, Computer, and Biomedical Engineering
Department of Chemical Engineering
University of Rhode Island
Kingston, RI 02881

Angelo Mao, Prof. David Mooney
Wyss Institute for Biologically Inspired Engineering
School of Engineering and Applied Sciences, Harvard University,
Cambridge, MA 02318, USA

Tian-Yun Huang, Prof. Xue-Bo Chen
School of Electronics and Information Engineering
Liaoning University of Science and Technology
Anshan, 114051, China

Keywords: microrobotics, micromachines, 3D printing, targeted drug and cell delivery, magnetism

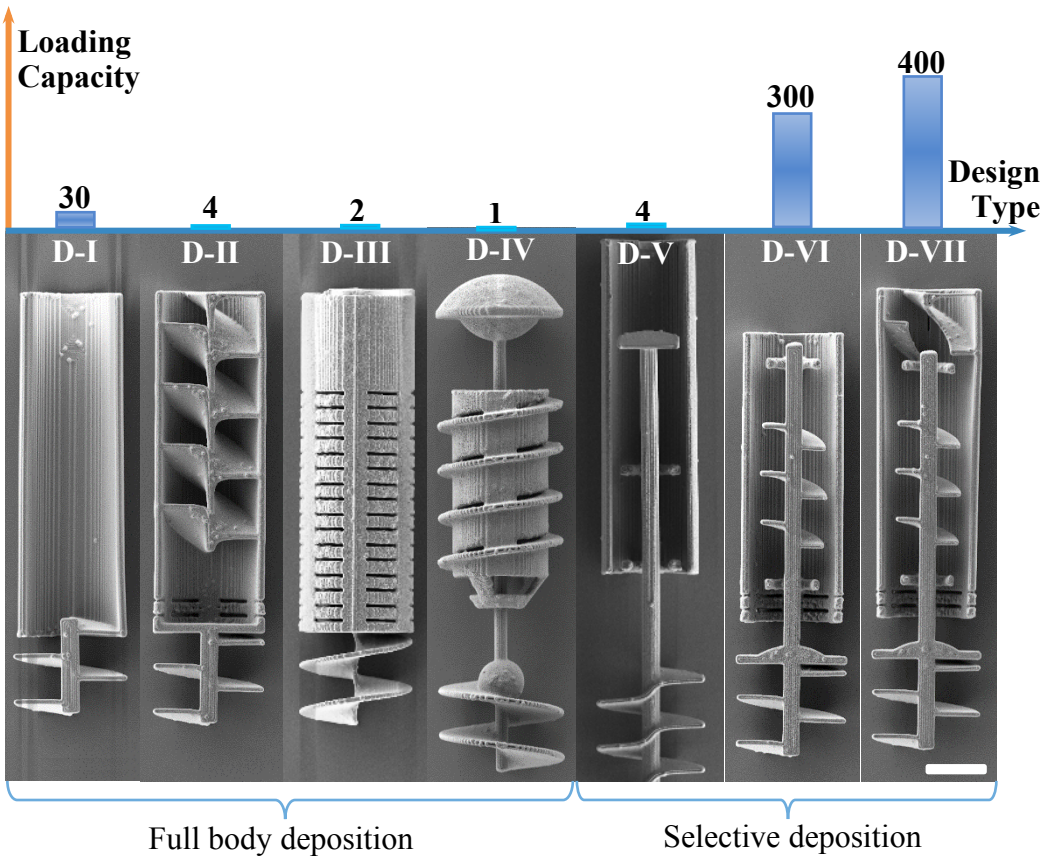

Figure S1. Comparative analysis of loading capacity of different prototypes. The bars show the average number of beads (3μm in diameter) that can be loaded into the devices. The scale bar is 20μm.

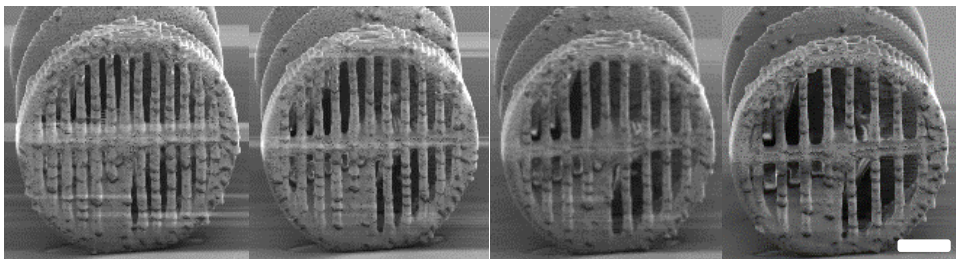

Figure S2. Apertures with different mesh sizes. The width of the holes are 1.521μm, 1.886μm, 2.270μm and 2.979μm, respectively The scale bar is 10μm.

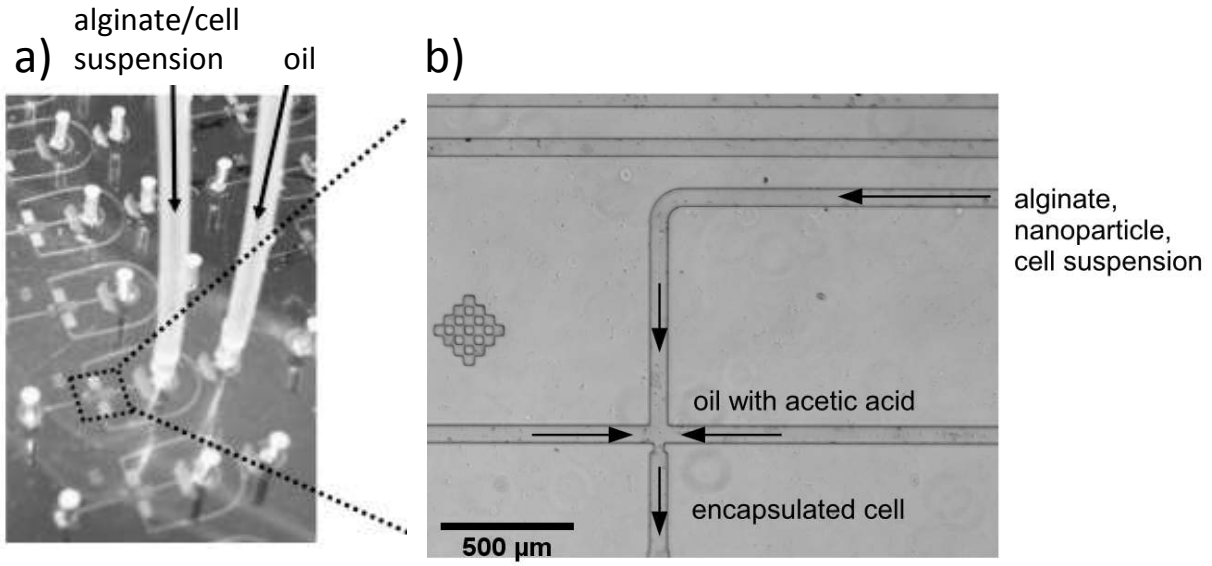

Figure S3. Illustration of the alginate cell-encapsulating microbead fabrication process. (a) A microbead precursor aqueous solution containing cells and oil are injected into a microfluidics device to generate cell-encapsulating microbeads. (b) Within the device, oil is used to pinch off micro-droplets of alginate. The scale bar is 500 µm. After being processed in the microfluidics device, micro-droplets are crosslinked using calcium chloride and removed from oil using 20% perfluorooctanol.

Table S1. Design parameters of micromachines (M), elongated apertures (A), helical microrobots (H) and microfluidic channels (C).

Design	M-I	M-II	A-I	H-I	C-I	C-II
Width (μm)	38.12	101.3	1.193	2.22	83.59	28.23
Length (μm)	176.3	664.0	9.030	5.33	500	500

Table of Contents Entry